Inorg. Chem. **2002**, *41*, 3191–3201

High-Nuclearity Sulfide-Rich Molybdenum–Iron–Sulfur Clusters: Reevaluation and Extension

Hong-Cai Zhou, Weiping Su, Catalina Achim, P. Venkateswara Rao, and R. H. Holm*

Department of Chemistry and Chemical Biology, Harvard University, Cambridge, Massachusetts 02138

Received February 12, 2002

High-nuclearity Mo–Fe–S clusters are of interest as potential synthetic precursors to the $MoFe_7S_9$ cofactor cluster of nitrogenase. In this context, the synthesis and properties of previously reported but sparsely described trinuclear $[(edt)_2M_2FeS_6]^{3-}$ (M = Mo (**2**), W (**3**)) and hexanuclear $[(edt)_2Mo_2Fe_4S_9]^{4-}$ (**4**, edt = ethane-1,2-dithiolate; Zhang, Z.; et al. *Kexue Tongbao* **1987**, *32*, 1405) have been reexamined and extended. More accurate structures of **2**–**4** that confirm earlier findings have been determined. Detailed preparations (not previously available) are given for **2** and **3**, whose structures exhibit the C_2 arrangement $\{[(edt)M(S)(\mu_2\text{-}S)_2]_2Fe^{III}\}^{3-}$ with square pyramidal Mo(V) and tetrahedral Fe(III). Oxidation states follow from ^{57}Fe Mössbauer parameters and an $S = {}^3/_2$ ground state from the EPR spectrum. The assembly system **2**/3$FeCl_3$/3Li_2S/*n*NaSEt in methanol/acetonitrile ($n = 4$) affords $(R_4N)_4$[**4**] (R = Et, Bu; 70–80%). The structure of **4** contains the $[Mo_2Fe_4(\mu_2\text{-}S)_6(\mu_3\text{-}S)_2(\mu_4\text{-}S)]^0$ core, with the same bridging pattern as the $[Fe_6S_9]^{2-}$ core of $[Fe_6S_9(SR)_2]^{4-}$ (**1**), in overall C_{2v} symmetry. Cluster **4** supports a reversible three-member electron transfer series 4–/3–/2– with $E_{1/2} = -0.76$ and –0.30 V in Me_2SO. Oxidation of $(Et_4N)_4$[**4**] in DMF with 1 equiv of tropylium ion gives $[(edt)_2Mo_2Fe_4S_9]^{3-}$ (**5**) isolated as $(Et_4N)_3$[**5**]·2DMF (75%). Alternatively, the assembly system ($n = 3$) gives the oxidized cluster directly as $(Bu_4N)_3$[**5**] (53%). Treatment of **5** with 1 equiv of $[Cp_2Fe]^{1+}$ in DMF did not result in one-electron oxidation but instead produced heptanuclear $[(edt)_2Mo_2Fe_5S_{11}]^{3-}$ (**6**), isolated as the Bu_4N^+salt (38%). Cluster **6** features the previously unknown core $Mo_2Fe_5(\mu_2\text{-}S)_7(\mu_3\text{-}S)_4$ in molecular C_2 symmetry. In **4**–**6**, the (edt)MoS_3 sites are distorted trigonal bipramidal and the FeS_4 sites are distorted tetrahedral with all sulfide ligands bridging. Mössbauer spectroscopic data for **2** and **4**–**6** are reported; (mean) iron oxidation states increase in the order **4** < **5** ≈ **1** < **6** ≈ **2**. Redox and spectroscopic data attributed earlier to clusters **2** and **4** are largely in disagreement with those determined in this work. The only iron and molybdenum–iron clusters with the same sulfide content as the iron–molybdenum cofactor of nitrogenase are $[Fe_6S_9(SR)_2]^{4-}$ and $[(edt)_2Mo_2Fe_4S_9]^{3-,4-}$.

Introduction

Clusters of the Fe−S and M−Fe−S types (M = Mo, V) whose nuclearity and sulfide content approach those of the native clusters of nitrogenase[1,2] are of interest as potential synthetic precursors to those clusters by atom addition or removal and skeletal rearrangement. The P-cluster and the iron−molybdenum cofactor (FeMoco) clusters have the core compositions $Fe_8S_7(\mu_2\text{-}S\cdot Cys)_2$ and $MoFe_7S_9$, respectively, and have been achieved only by biosynthesis.[3−5] Compositions and structures are definitively established for the P-cluster and FeMoco by protein crystallography.[6,7] Several lines of evidence, including EXAFS results,[8−10] are consistent

* Author to whom correspondence should be addressed. E-mail: holm@chemistry.harvard.edu.

(1) Howard, J. B.; Rees, D. C. *Chem. Rev.* **1996**, *96*, 2965−2982.
(2) Smith, B. E. *Adv. Inorg. Chem.* **1999**, *47*, 160−218.
(3) Dean, D. R.; Jacobson, M. R. In *Biological Nitrogen Fixation*; Stacey, G., Burris, R. H., Evans, H. J., Eds.; Chapman & Hall: New York, 1992; pp 763−834.
(4) Ludden, P. W.; Shah, V. K.; Roberts, G. P.; Rüttimann-Johnson, C.; Rangaraj, P.; Foulger, T.; Allen, R. M.; Homer, M.; Roll, J. T.; Zhang, X.; Chatterjee, R. In *Biological Nitrogen Fixation for the 21st Century*; Kondorosi, A., Newton, W. E., Eds.; Kluwer: Boston, 1998; pp 33−38.
(5) Ribbe, M. W.; Burgess, B. K. *Proc. Natl. Acad. Sci. U.S.A.* **2001**, *98*, 5521−5525.
(6) Peters, J. W.; Stowell, M. H. B.; Soltis, S. M.; Finnegan, M. G.; Johnson, M. K.; Rees, D. C. *Biochemistry* **1997**, *36*, 1181−1187.
(7) Mayer, S. M.; Lawson, D. M.; Gormal, C. A.; Roe, S. M.; Smith, B. E. *J. Mol. Biol.* **1999**, *292*, 871−891.
(8) George, G. N.; Coyle, C. L.; Hales, B. J.; Cramer, S. P. *J. Am. Chem. Soc.* **1988**, *110*, 4057−4059.

10.1021/ic0201250 CCC: $22.00
Published on Web 05/17/2002

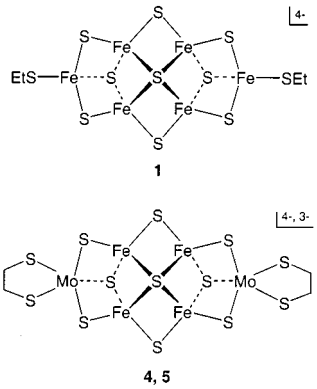

Figure 1. Structures of the two types of high-nuclearity iron−sulfur and molybdenum−iron−sulfur clusters that contain nine sulfide atoms: $[Fe_6S_9(SEt)_2]^{4-}$ (**1**) and $[(edt)_2Mo_2Fe_4S_9]^{4-,3-}$ (**4**, **5**).

with a similar or identical structure for FeVco from vanadium nitrogenase.[2,11] The FeFeco from iron-only nitrogenase[2,12] is believed to be structurally homologous to FeMoco on the basis of biochemical and genetics considerations and spectroscopic results.[13]

In the development of iron−sulfur−thiolate/halide cluster chemistry, the first example of a cluster with a nuclearity higher than that of the familiar Fe_4S_4 cubane-type species was $[Fe_6S_9(SR)_2]^{4-}$,[14−18] which contains the unusual $[Fe_6(\mu_2\text{-}S)_6(\mu_3\text{-}S)_2(\mu_4\text{-}S)]^{2-}$ core of idealized C_{2v} symmetry with the μ_4-S and μ_3-S atoms above and below the Fe_6 plane. One example, $[Fe_6S_9(SEt)_2]^{4-}$, is depicted as **1** in Figure 1. Thereafter, the isostructural mixed ligand cluster $[Fe_6S_9(SCH_2CH_2OH)Cl]^{4-}$ was reported.[19,20] Other structural types are represented by the prismanes $[Fe_6S_6L_6]^{2-,3-}$ (L = RO^-, RS^-, halide)[21−23] and the double cubane $\{[Fe_4S_4Cl_3]_2(\mu_2\text{-}S)\}^{4-}$.[24] These and other octanuclear species with heterometallic cores $\{[MoFe_3S_4]_2(\mu_2\text{-}S)\}^{4+}$ have been prepared and investigated as precursors to clusters related to those in nitrogenase.[25−27] Recently, we have shown that the edge-bridged double cubane $[(Cl_4cat)_2(Et_3P)_2Mo_2Fe_6S_8(PEt_3)_4]$[28,29] serves as a starting material in reactions that afford larger clusters containing the core fragment $Mo_2Fe_6S_9$.[30,31] (Abbreviations are given in Chart 1.) This fragment is a close topological analogue of the nitrogenase P^N cluster. In a new development, Han and Coucouvanis[32] describe a double cubane with an intercube Fe−(μ_3-S) bond and a total core composition of $Mo_2Fe_6S_8$.

Chart 1. Designation of Clusters[a,b]

$[Fe_6S_9(SEt)_2]^{4-}$	**1**[16]
$[(edt)_2Mo_2FeS_6]^{3-}$	**2**[34-40]
$[(edt)_2W_2FeS_6]^{3-}$	**3**[35,41]
$[(edt)_2Mo_2Fe_4S_9]^{4-}$	**4**[33-35]
$[(edt)_2Mo_2Fe_4S_9]^{3-}$	**5**
$[(edt)_2Mo_2Fe_5S_{11}]^{3-}$	**6**

[a] Abbreviations: Cl_4cat = tetrachlorocatecholate(2−), edt = ethane-1,2-dithiolate(2−), TCNQ = 7,7,8,8-tetracyanoquinodimethane. [b] In these and other formulas, terminal ligands bound to the heterometal precede Mo or W.

In the foregoing context, in which clusters whose metal and/or sulfide contents approach or achieve eight and nine, respectively, we have become concerned with the heterometallic hexanuclear cluster described as $[(edt)_2Mo_2Fe_4S_9]^{4-}$ and first reported in 1987 as its Et_4N^+ salt by Zhang et al.[33] Additional reports of structure and certain physical properties followed in 1988−1989.[34,35] This cluster has the same sulfide content but two fewer metal atoms than FeMoco. Remarkably, the cluster (**4**, Figure 1) has the same core bridging pattern as does $[Fe_6S_9(SR)_2]^{4-}$, with two Mo(edt) ring fragments in place of Fe−SR at the termini of the cluster. This fragment, with two sulfide bridges to an iron atom, is present in trinuclear $[(edt)_2Mo_2FeS_6]^{3-}$, first prepared by Dahlstrom et al. in 1981,[36] who established the linear trinuclear structure **2** shown in Figure 2. Thereafter, the cluster was reprepared and its structure determined in several different crystals, mainly by the same group that reported **4**, and several of its properties were described.[34,35,37−40] The

(9) Arber, J. M.; Dobson, B. R.; Eady, R. R.; Hasnain, S. S.; Garner, C. D.; Matsushita, T.; Nomura, M.; Smith, B. E. *Biochem. J.* **1989**, *258*, 733−737.
(10) Chen, J.; Christiansen, J.; Tittsworth, R. C.; Hales, B. J.; George, S. J.; Coucouvanis, D.; Cramer, S. P. *J. Am. Chem. Soc.* **1993**, *115*, 5509−5515.
(11) Eady, R. R. *Chem. Rev.* **1996**, *96*, 3013−3030.
(12) Schneider, K.; Gollan, U.; Dröttboom, M.; Selsemeier-Voigt, S.; Müller, A. *Eur. J. Biochem.* **1997**, *244*, 789−800.
(13) Krahn, E.; Weiss, B. J. R.; Kröckel, M.; Groppe, J.; Henkel, G.; Cramer, S. P.; Trautwein, A. X.; Schneider, K.; Müller, A. *J. Biol. Inorg. Chem.* **2002**, *7*, 37−45.
(14) Christou, G.; Holm, R. H.; Sabat, M.; Ibers, J. A. *J. Am. Chem. Soc.* **1981**, *103*, 6269−6271.
(15) Christou, G.; Sabat, M.; Ibers, J. A.; Holm, R. H. *Inorg. Chem.* **1982**, *21*, 3518−3526.
(16) Hagen, K. S.; Watson, A. D.; Holm, R. H. *J. Am. Chem. Soc.* **1983**, *105*, 3905−3913.
(17) Henkel, G.; Strasdeit, H.; Krebs, B. *Angew. Chem., Int. Ed. Engl.* **1982**, *21*, 201−202.
(18) Strasdeit, H.; Krebs, B.; Henkel, G. *Inorg. Chem.* **1984**, *23*, 1816−1825.
(19) Zhang, Z.; Liu, X.; Fan, Y. *Kexue Tongbao* **1985**, *30*, 1351−1354.
(20) Fan, Y.; Guo, C.; Zhang, Z.; Liu, X. *Sci. Sin., Ser. B* **1988**, *31*, 161−170.
(21) Coucouvanis, D.; Kanatzidis, M. G.; Dunham, W. R.; Hagen, W. R. *J. Am. Chem. Soc.* **1984**, *106*, 7998−7999.
(22) Kanatzidis, M. G.; Hagen, W. R.; Dunham, W. R.; Lester, R. K.; Coucouvanis, D. *J. Am. Chem. Soc.* **1985**, *107*, 953−961.
(23) Kanatzidis, M. G.; Salifoglou, A.; Coucouvanis, D. *Inorg. Chem.* **1986**, *25*, 2460−2468.
(24) Challen, P. R.; Koo, S. M.; Dunham, W. R.; Coucouvanis, D. *J. Am. Chem. Soc.* **1990**, *112*, 2455−2456.
(25) Huang, J.; Mukerjee, S.; Segal, B. M.; Akashi, H.; Zhou, J.; Holm, R. H. *J. Am. Chem. Soc.* **1997**, *119*, 8662−8674.
(26) Huang, J.; Holm, R. H. *Inorg. Chem.* **1998**, *37*, 2247−2254.
(27) Fomitchev, D. V.; McLauchlan, C. C.; Holm, R. H. *Inorg. Chem.* **2002**, *41*, 958−966.
(28) Demadis, K. D.; Campana, C. F.; Coucouvanis, D. *J. Am. Chem. Soc.* **1995**, *117*, 7832−7833.
(29) Osterloh, F.; Segal, B. M.; Achim, C.; Holm, R. H. *Inorg. Chem.* **2000**, *39*, 980−989.
(30) Osterloh, F.; Sanakis, Y.; Staples, R. J.; Münck, E.; Holm, R. H. *Angew. Chem., Int. Ed.* **1999**, *38*, 2066−2070.
(31) Osterloh, F.; Achim, C.; Holm, R. H. *Inorg. Chem.* **2001**, *40*, 224−232.
(32) Han, J.; Coucouvanis, D. *J. Am. Chem. Soc.* **2001**, *123*, 11304−11305.
(33) Zhang, Z.; Fan, Y.; Li, Y.; Niu, S.; Li, S. *Kexue Tongbao* **1987**, *32*, 1405−1409.
(34) Niu, S.; Zhang, Z.; Pan, M.; Jiang, Y.; Wang, T.; Lin, X. *Kexue Tongbao* **1988**, *33*, 27−31.
(35) Zhang, Z.; Sun, W.; Niu, S.; Li, S.; Ye, L.; Fan, Y.; Guo, C. *Wuji Huaxue Xuebao* **1989**, *5*, 35−42.
(36) Dahlstrom, P. L.; Kumar, S.; Zubieta, J. *J. Chem. Soc., Chem. Commun.* **1981**, 411−412.
(37) Wang, F.; Zhang, Z.; Fan, Y.; Shen, C. *Jilin Daxue Ziran Kexue Xuebao* **1984**, 94−98.
(38) Zhang, Z.; Wang, F.; Fan, Y. *Kexue Tongbao* **1984**, *29*, 1486−1489.

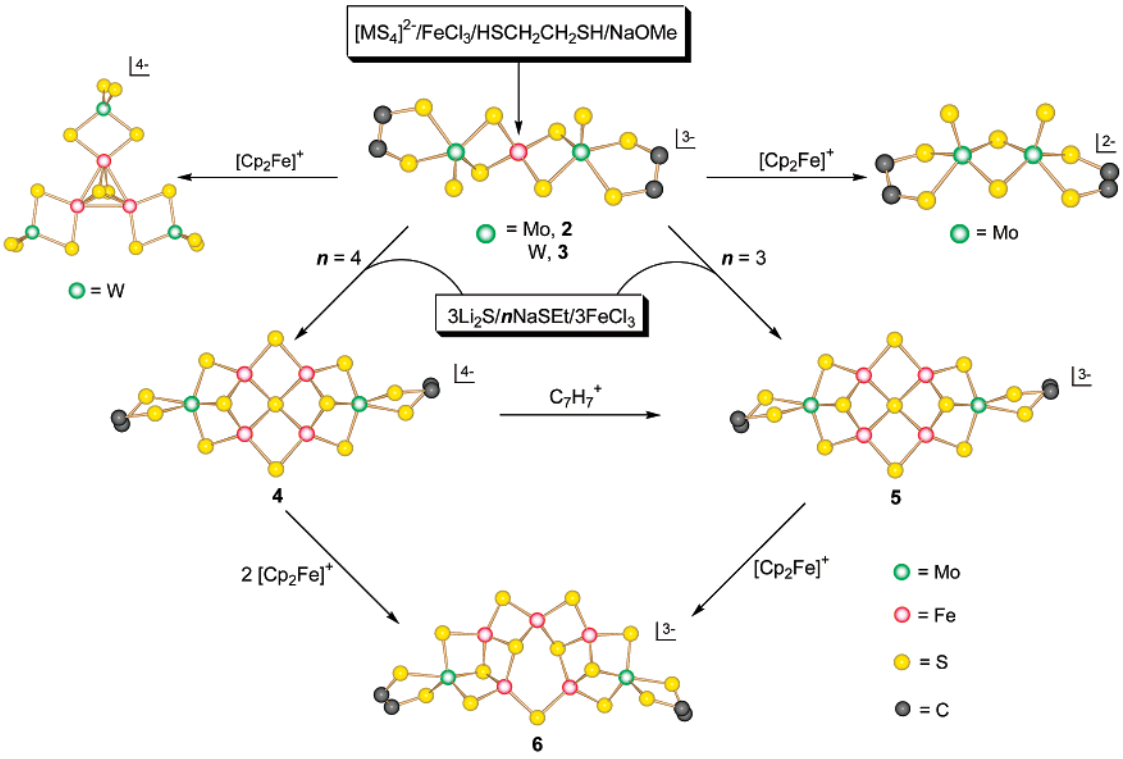

Figure 2. Synthetic scheme for $[(edt)_2M_2FeS_6]^{3-}$ (M = Mo (**2**), W (**3**)), $[(edt)_2Mo_2Fe_4S_9]^{4-}$ (**4**), $[(edt)_2Mo_2Fe_4S_9]^{3-}$ (**5**), and $[(edt)_2Mo_2Fe_5S_{11}]^{3-}$ (**6**). Also shown are $[(edt)_2Mo_2S_4]^{2-}$ and $[W_3Fe_3S_{14}]^{4-}$, formed in the oxidation of **2** and **3**, respectively.

isostructural cluster $[(edt)_2W_2FeS_6]^{3-}$ (**3**) has also been obtained.[35,41] Consideration of the preparative method led us to the possibility that **2** is a synthetic precursor of **4**. Further, some of the properties reported for **2** and **4** are not those expected on the basis of our experience in Mo−Fe−S cluster chemistry. We have reinvestigated the synthesis and properties of these clusters and have found substantial differences, and a larger scope to the chemistry than might have been supposed from the reported information. The principal results of that investigation are set out here as our initial study of structure type **4** and other clusters related thereto.

Experimental Section

Preparation of Compounds. All operations were conducted under a pure dinitrogen atmosphere using an inert atmosphere box or standard Schlenk techniques. Solvents were passed through an Innovative Technology solvent purification system prior to use. Previous descriptions of the preparations of salts of clusters **2**−**4** have been brief, often without specifying mole ratios of reactants, conditions, or yields. We include detailed preparations of these and two other clusters including elemental analyses and selected properties for secure identification. The compound $(Et_4N)_4[Fe_6S_9(SEt)_2]$ was prepared as described.[16]

$(Et_4N)_3[(edt)_2Mo_2FeS_6]$. To a solution of 10.4 g (192 mmol) of NaOMe in 360 mL of methanol was added 8.22 mL (98 mmol) of ethane-1,2-dithiol. The solution of $Na_2(edt)$ was treated with a suspension of 6.25 g (24.0 mmol) of $(NH_4)_2[MoS_4]$ in 50 mL of methanol with stirring. To the reaction mixture was introduced a filtered solution of 1.95 g (12.0 mmol) of $FeCl_3$ in 50 mL of methanol, giving a black suspension. The mixture was stirred overnight, and the dark red-brown solution obtained was filtered into a solution of 5.97 g (36.0 mmol) of Et_4NCl in 50 mL of methanol to precipitate a black crystalline solid. The reaction mixture was maintained at −20 °C overnight to crystallize more product. The solid was collected by filtration, washed with 3 × 10 mL of acetonitrile/ether (1:1 v/v) and 3 × 5 mL of ether, and dried. It was placed on a frit and extensively extracted with warm (55 °C) acetonitrile. The extract was concentrated until solid began to appear and carefully layered with ether (500 mL). The mixture was allowed to stand at −20 °C for 12 h, during which a black crystalline solid separated. The solid was collected by filtration, washed with ether, and dried in a vacuum to afford 9.8 g (80%) of product pure by an NMR criterion. The compound is soluble in acetonitrile, DMF, Me_2SO, and water. Absorption spectrum (DMF): λ_{max} (ϵ_M) 307 (30000), 365 (22200), 389 (21700), 473 (9600), 576 (6680), 697 (1260) nm. ^1H NMR (D_2O, anion): δ 35.5 (1), 31.8 (1), 30.8 (1), 20.3 (1); (CD_3CN, anion) δ 36.9 (1), 34.9 (1), 29.8 (1), 22.8 (1). Anal. Calcd for $C_{28}H_{68}FeMo_2N_3S_{10}$: C, 33.13; H, 6.75; Fe, 5.50; Mo, 18.90; N, 4.14; S, 31.58. Found: C, 33.02; H, 6.70; Fe, 5.57; Mo, 18.76; N, 4.17; S, 31.44.

$(Bu_4N)_3[(edt)_2Mo_2FeS_6]$. A solution of 40.0 mmol of $Na_2(edt)$ in 80 mL of methanol (from ethane-1,2-dithiol and NaOMe) was added to a suspension of 2.60 g (9.99 mmol) of $(NH_4)_2[MoS_4]$ in 20 mL of methanol, resulting in a deep red solution. A filtered solution of 0.81 g (4.99 mmol) of $FeCl_3$ in 20 mL of methanol was added, and the reaction mixture was stirred for 20 h. The mixture was filtered into a solution of 4.87 g (15.1 mmol) of Bu_4NBr in a minimal volume of methanol, the volume was concentrated to ca.100 mL, and the mixture was maintained at −20 °C overnight to afford a black crystalline solid. This material was collected by filtration and extensively extracted with acetonitrile until a pale-

(39) Zhang, Z.; Fan, Y. *Jilin Daxue Ziran Kexue Xuebao* **1988**, 97−103.
(40) Ng, S. W.; Hu, S.-Z. *Chin. J. Struct. Chem.* **2000**, *19*, 405−410.
(41) Wu, L.; Fan, Y.; Zhang, Z.; Guo, C. *Jilin Daxue Ziran Kexue Xuebao* **1991**, 93−97.

colored solid remained. The extracts were combined, reduced in volume, layered with ether, and stored at −20 °C overnight. The product was obtained as 4.75 g (70%) of black crystalline product. The compound is soluble in polar organic solvents. The absorption and ^{1}H NMR spectrum are identical to those of the Et_4N^+ salt.

$(Et_4N)_3[(edt)_2W_2FeS_6]$. A filtered solution of 0.649 g (4.00 mmol) of $FeCl_3$ in 20 mL of methanol was added to a solution of 24.0 mmol of Na_2(edt) in 150 mL of methanol. The dark brown-red solution was stirred for 30 min, and 1.96 g (8.00 mmol) of $(NH_4)_2[WS_4]$ was added. The reaction mixture was stirred and heated at 55 °C for 22 h, cooled, and filtered into solution of 2.00 g (12.0 mmol) of Et_4NCl in 5 mL of methanol. The mixture was filtered, and the filtrate was reduced to 90 mL and maintained at −20 °C overnight. A mixture of black crystalline solid and a yellowish solid was collected by filtration and extracted with acetonitrile (total 175 mL) until all the black solid dissolved. The extract was concentrated to 120 mL and layered with 350 mL of ether. Upon standing the product was collected by filtration, washed with ether, and dried to afford 1.73 g (36%) of black crystalline solid. Absorption spectrum (DMF): λ_{max} (ϵ_M) 298 (26600), 365 (23400), 412 (9760), 513 (7950), 579 (1730) nm. ^{1}H NMR (CD_3CN, anion): δ 33.4 (1), 31.0 (1), 27.7 (1), 21.2 (1). Anal. Calcd for $C_{28}H_{68}FeN_3S_{10}W_2$: C, 28.24; H, 5.75; Fe, 4.69; N, 3.53; S, 26.92; W, 30.87. Found: C, 28.40; H, 5.68; Fe, 4.76; N, 3.62; S, 26.85; W, 30.81.

$(Et_4N)_4[(edt)_2Mo_2Fe_4S_9]\cdot x$LiCl. The compounds NaSEt (1.02 g, 12.1 mmol) and Li_2S (0.42 g, 9.0 mmol) were dissolved in 40 mL of methanol, and a filtered solution of 1.46 g (9.00 mmol) of $FeCl_3$ in 20 mL of methanol was added, followed by the addition of a suspension of 3.05 g (3.00 mmol) of $(Et_4N)_3[(edt)_2Mo_2FeS_6]$ in 70 mL of acetonitrile. The dark brown reaction mixture was stirred for 18 h and added to a solution of 0.50 g (3.00 mmol) of Et_4NCl in 5 mL of methanol. The mixture was stirred for 6 h, the black suspension was filtered, and the filtrate was layered on top of THF (350 mL) to precipitate a fine microcrystalline black solid. This material was collected by filtration, washed with THF, acetonitrile, and ether (each 3 × 10 mL), and dried in vacuum overnight to yield 3.25 g (60%) of product. This material can be further purified by recrystallization from Me_2SO/ether as black flakelike crystals or from NMF/ether as black needlelike crystals. ^{1}H NMR (Me_2SO, anion): δ 6.65 (br); (D_2O, anion) δ 7.35 (br). Despite considerable effort, we were unable to achieve a separation of the product compound from LiCl. Analytical data are in satisfactory agreement with $x = 5$. Anal. Calcd. for $C_{36}H_{88}Fe_4Mo_2N_4S_{13}\cdot 5$LiCl: C, 26.67; H, 5.47; Fe, 13.78; Mo, 11.84; N, 3.46; S, 25.71. Found: C, 26.50; H, 5.26; Fe, 13.67; Mo, 11.75; N, 3.42; S, 25.91.

$(Bu_4N)_4[(edt)_2Mo_2Fe_4S_9]$. Method A. Initially isolated $(Et_4N)_4[(edt)_2Mo_2Fe_4S_9]\cdot 5$LiCl (0.80 g, 0.49 mmol) was placed on a frit and extracted with degassed water (10 mL). The filtrate was added slowly to an aqueous solution of $(Bu_4N)Br$ (8.0 g, 25 mmol) with vigorous stirring. The black precipitate which appeared immediately was collected by filtration, washed with water, and dried under vacuum overnight. Recrystallization from acetonitrile/ether afforded the product as 0.50 g (55%) of black fiberlike crystals. ^{1}H NMR (CD_3CN, anion): δ 6.91 (br). Absorption spectrum (DMF): λ_{max} (ϵ_M) 334 (70500), 516 (18600) nm.

Method B. The compounds NaSEt (0.280 g, 3.33 mol) and Li_2S (0.102 g, 2.22 mmol) were dissolved in 15 mL of methanol, and a filtered solution of 0.360 g (2.22 mmol) of $FeCl_3$ in 5 mL of methanol was added, followed by the addition of a solution of 1.00 g (0.74 mmol) of $(Bu_4N)_3[(edt)_2Mo_2FeS_6]$ in 15 mL of acetonitrile. The dark brown reaction mixture was stirred for 20 h and added to a solution of 0.238 g (0.74 mmol) of Bu_4NBr in 5 mL of methanol. The reaction mixture was stirred for 4 h and filtered, and the filtrate was layered on top of THF (350 mL). The black solid was collected by filtration, washed with THF and ether, and dried in vacuo to yield 0.69 g (58%) of product. This material may be further purified by recrystallization from acetonitrile/ether. The absorption and ^{1}H NMR spectra are identical to those of the product of method A.

$(Bu_4N)_3[(edt)_2Mo_2Fe_4S_9]$. To a solution of 0.21 g (4.66 mmol) of Li_2S and 0.39 g (4.65 mmol) of NaSEt in 18 mL of methanol was added a filtered solution of 0.76 g (4.66 mmol) of $FeCl_3$ in 5 mL of methanol and a solution of 2.10 g (1.55 mmol) of $(Bu_4N)_3[(edt)_2Mo_2FeS_6]$ in 18 mL of acetonitrile. The reaction mixture was stirred overnight and filtered to remove a small amount of black solid. The filtrate was reduced to dryness and washed extensively with THF. The solid was dissolved in 40 mL of acetonitrile, and the solution was filtered and layered with 300 mL of ether. Upon standing, a solid separated, which was collected, washed with ether, and dried to give the product as 1.33 g (53%) of black crystalline solid. ^{1}H NMR (CD_3CN, anion): δ 12.2. Anal. Calcd for $C_{52}H_{116}Fe_4Mo_2N_3S_{13}$: C, 38.66; H, 7.24; Fe, 13.83; Mo, 11.88; N, 2.60; S, 25.80. Found: C, 38.54; H, 7.29; Fe, 13.77; Mo, 11.13; N, 2.56; S, 25.76.

$(Et_4N)_3[(edt)_2Mo_2Fe_4S_9]\cdot 2$DMF. A suspension of 0.637 g (0.394 mmol) of $(Et_4N)_4[(edt)_2Mo_2Fe_4S_9]\cdot 5$LiCl in 10 mL of DMF was treated with a solution of 0.080 g (0.450 mmol) of tropylium tetrafluoroborate in 5 mL of DMF. The reaction mixture was stirred for 3 h; the dark red solution was filtered through a Celite column to remove a dark solid. Vapor diffusion of ether into the filtrate caused separation of the product as 0.16 g (75%) of black shiny flakes. Absorption spectrum (DMF): λ_{max} (ϵ_M) 354 (42800), 520 (14100) nm. ^{1}H NMR (Me_2SO, anion): δ 12.6 (1), 10.6 (1). Anal. Calcd for $C_{34}H_{82}Fe_4Mo_2N_5O_2S_{13}$: C, 28.66; H, 5.80; Fe, 15.68; Mo, 13.46; N, 4.91; S, 29.25. Found: C, 28.78; H, 5.75; Fe, 15.76; Mo, 13.39; N, 5.03; S, 29.18.

$(Bu_4N)_3[(edt)_2Mo_2Fe_5S_{11}]$. The compound $(Bu_4N)_3[(edt)_2Mo_2Fe_4S_9]$ (0.520 g, 0.322 mmol) was dissolved in 10 mL of DMF and was treated with a solution of 0.106 g (0.320 mmol) of $[Cp_2Fe](PF_6)$ in 3 mL of DMF. The reaction mixture was stirred for 3 h and filtered through a Celite pad. Vapor diffusion of ether into the filtrate caused separation of a black solid, which was collected by filtration, washed with ether, and extracted by stirring overnight with 15 mL of acetonitrile. The solution was filtered to remove an insoluble black residue, and Bu^tOMe was layered onto the filtrate, causing separation of the product as 0.21 g (38%) of a microcrystalline black solid. Absorption spectrum (DMF): λ_{max} (ϵ_M) 358 (40700), 509 (sh, 18900) nm. ^{1}H NMR (CD_3CN, anion): δ 6.49 (br). Anal. Calcd for $C_{52}H_{116}Fe_5Mo_2N_3S_{15}$: C, 35.99; H, 6.74; Fe, 16.09; Mo, 11.06; N, 2.42; S, 27.71. Found: C, 35.76; H, 6.67; Fe, 16.18; Mo, 11.65; N, 2.41; S, 27.66.

$(Et_4N)_3[(edt)_2Mo_2Fe_5S_{11}]\cdot 2$DMF. A suspension of 0.113 g (0.081 mmol) of $(Et_4N)_4[(edt)_2Mo_2Fe_4S_9]$ in 2 mL of DMF was treated with 1 mL of a solution of 53.3 mg (0.161 mmol) of $[Cp_2Fe](PF_6)$ in 2 mL of DMF. The dark red solution was stirred for 90 min and a second milliliter of the ferrocenium solution added. Stirring was continued for 90 min, the solution was filtered through Celite, and the filtrate was carefully layered with ether. After 3 days, the product was collected as 55 mg (44%) of black crystalline solid. ^{1}H NMR (Me_2SO, anion): δ 6.28 (br). This compound was identified by an X-ray structure determination.

Oxidation of $[(edt)_2M_2FeS_6]^{3-}$. (a) M = Mo. To a solution of 0.209 g (0.206 mmol) of $(Et_4N)_3[(edt)_2Mo_2FeS_6]$ in 2 mL of DMF was added 0.060 g (0.18 mmol) of $[Cp_2Fe](PF_6)$ in 1 mL of DMF.

Table 1. Crystallographic Data[a]

	$(Et_4N)_3$[**2**]	$(Et_4N)_3$[**3**]	$(Et_4N)_4$[**4**]	$(Et_4N)_4$[**4**]
formula	$C_{28}H_{68}FeMo_2N_3S_{10}$	$C_{28}H_{68}FeN_3S_{10}W_2$	$C_{36}H_{88}Fe_4Mo_2N_4S_{13}$	$C_{36}H_{88}Fe_4Mo_2N_4S_{13}$
cryst syst	monoclinic	monoclinic	monoclinic	orthorhombic
fw	1015.18	1191.00	1409.16	1409.16
space group	*C*2/*c*	*C*2/*c*	*C*2/*c*	$Pna2_1$
a, Å	13.705(2)	13.668(3)	17.8927(9)	19.054(1)
b, Å	18.404(2)	18.355(4)	34.137(2)	17.660(1)
c, Å	17.502(2)	17.482(3)	12.5379(6)	17.318(1)
β, deg	101.551(4)	101.382(4)	127.968(1)	
V, Å^3	4325.1(8)	4230(1)	6037.4(5)	5827.3(6)
Z	4	4	4	4
ρ_{calcd}, g cm^{-3}	1.559	1.840	1.550	1.606
2θ range, deg	3.76−56.6	3.76−49.6	3.14−45.0	3.14−45.0
GOF (F^2)	1.022	0.995	1.077	1.099
R1[b,d]/R1[c,d]	0.0252/0.0292	0.0364/0.0466	0.058/0.076	0.064/0.082
wR2[b,e]/wR2[c,e]	0.0727/0.0743	0.0855/0.0907	0.145/0.157	0.145/0.157

[a] Obtained with graphite-monochromatized Mo Kα ($\lambda = 0.71071$ Å) radiation at 213 K. [b] Denotes value of the residual considering only the reflections with $I > 2\sigma(I)$. [c] Denotes value of the residual considering all the reflections. [d] $R1 = \sum(|F_o| - |F_c|)/\sum|F_o|$. [e] $wR2 = \{\sum[w(F_o^2 - F_c^2)^2]/\sum[w(F_o^2)^2]\}^{1/2}$; $w = 1/[\sigma^2(F_o^2) + (aP)^2 + bP]$, $P = [\max(F_o^2 \text{ or } 0) + 2(F_c^2)]/3$.

Table 2. Crystallographic Data[a]

	$(Et_4N)_3$[**5**]·2DMF	$(Bu_4N)_3$[**5**]·DMF	$(Et_4N)_3$[**6**]·2DMF
formula	$C_{34}H_{82}Fe_4Mo_2N_5O_2S_{13}$	$C_{55}H_{123}Fe_4Mo_2N_4OS_{13}$	$C_{34}H_{82}Fe_5Mo_2N_5O_2S_{15}$
cryst syst	monoclinic	monoclinic	monoclinic
fw	1425.11	1688.63	1545.08
space group	*C*2/*c*	*C*2/*c*	$P2_1/n$
a, Å	10.520(2)	16.725(2)	10.013(1)
b, Å	17.153(4)	11.760(2)	32.172(3)
c, Å	32.639(7)	40.348(6)	19.037(2)
β, deg	98.833(4)	93.105(2)	92.815(2)
V, Å^3	5820(2)	7924(2)	6125(1)
Z	4	4	4
ρ_{calcd}, g cm^{-3}	1.627	1.415	1.676
2θ range, deg	2.52−45.0	4.32−45.0	2.48−56.68
GOF (F^2)	1.217	1.134	0.981
R1[b,d]/R1[c,d]	0.089/0.096	0.0654/0.0921	0.053/0.078
wR2[b,e]/wR2[c,e]	0.215/0.219	0.132/0.144	0.141/0.150

[a] Obtained with graphite-monochromatized Mo Kα ($\lambda = 0.71071$ Å) radiation at 213 K. [b] Denotes value of the residual considering only the reflections with $I > 2\sigma(I)$. [c] Denotes value of the residual considering all the reflections. [d] $R1 = \sum(|F_o| - |F_c|)/\sum|F_o|$. [e] $wR2 = \{\sum[w(F_o^2 - F_c^2)^2]/\sum[w(F_o^2)^2]\}^{1/2}$; $w = 1/[\sigma^2(F_o^2) + (aP)^2 + bP]$, $P = [\max(F_o^2 \text{ or } 0) + 2(F_c^2)]/3$.

The deep brown solution was stirred for 3 h and filtered through a Celite column. Vapor diffusion of ether into the filtrate caused separation of an orange crystalline product. This material was identified by comparison of cell parameters and solution of the structure as $(Et_4N)_2[Mo_2S_4(edt)_2]$ (0.084 g, 55%) with the anion in the syn configuration.[42−44]

(b) M = W. A suspension of 0.670 g (0.562 mmol) of $(Et_4N)_3[(edt)_2W_2FeS_6]$ in 6 mL of DMF was treated with a solution of 0.186 g (0.562 mmol) $[Cp_2Fe](PF_6)$ in 3 mL of DMF. The solution was filtered through a Celite column. Vapor diffusion of ether into the filtrate resulted in a sticky mass, which was dissolved in Me_2SO. Vapor diffusion of THF into the Me_2SO solution resulted in formation of a black solid, identified by its absorption spectrum, comparison of cell parameters, and structure determination as $(Et_4N)_4[W_3Fe_3S_{14}]$[45] (26%).

In the sections which follow, clusters are numerically designated according to Chart 1.

X-ray Structure Determinations. Data were collected on a Siemens (Bruker) SMART CCD-based diffractometer; crystals were mounted on glass fibers and maintained under a stream of dinitrogen at 213 K. Cell parameters were retrieved using SMART software and refined using SAINT on all observed reflections. Data were collected using 0.3° intervals in φ and ω for 30 s/frame such that a hemisphere of data was collected. A total of 1271 frames was collected with a maximum resolution of 0.75 Å. The first 50 frames were re-collected at the end of the data collection to monitor for decay; none was found. The highly redundant data sets were reduced using SAINT and corrected for Lorentz and polarization effects. Absorption corrections were applied using SADABS supplied by Bruker.

Structures were solved by direct methods using the program SHELXL-97. The positions of the metal atoms and their first coordination spheres were located from direct-methods *E*-maps; other non-hydrogen atoms were found in alternating difference Fourier syntheses and least-squares refinement cycles and, during the final cycles, refined anisotropically. Hydrogen atoms were placed in calculated positions employing a riding model with thermal parameters 1.2 times those of the bonded carbon atoms for all methylene groups, and 1.5 times for methyl groups. If necessary, high angle data were deleted during the final least-squares refinement cycles. Crystallographic data are given in Tables 1 and 2. Disordered Et_4N^+ cations were found in all structures; each of them was modeled successfully as having two orientations with approximately half-occupancy for each orientation.

(42) Bunzey, G.; Enemark, J. H.; Howie, J. K.; Sawyer, D. T. *J. Am. Chem. Soc.* **1977**, *99*, 4168−4170.
(43) Bunzey, G.; Enemark, J. H. *Inorg. Chem.* **1978**, *17*, 682−688.
(44) Miller, K. F.; Bruce, A. E.; Corbin, J. L.; Wherland, S.; Stiefel, E. I. *J. Am. Chem. Soc.* **1980**, *102*, 5102−5104.
(45) Müller, A.; Hellman, W.; Bögge, H.; Jostes, R.; Römer, M.; Schimanski, U. *Angew. Chem., Int. Ed. Engl.* **1982**, *21*, 860−861.

Black square plates of $(Et_3N)_3$[**2**] were grown by acetonitrile/ether vapor diffusion. The compound crystallizes in monoclinic space group $C2/c$ with $Z = 4$. The asymmetric unit contains one-half cluster anion, and one and a half cations. The iron atom resides on a 2-fold axis and the nitrogen atom of the half-cation resides on an inversion center. Black blocks of $(Et_3N)_3$[**3**] were obtained by NMF/ether vapor diffusion. The crystal structures of $(Et_4N)_3$[**2**] and $(Et_4N)_3$[**3**] are isotypic. Black needles and plates of $(Et_4N)_4$[**4**] were grown from Me_2SO/Bu^{t}OMe vapor diffusion; the plates crystallize in monoclinic space group $C2/c$ with $Z = 4$. The asymmetric unit consists of one-half cluster anion and two cations. Black needles were also isolated from NMF/ether vapor diffusion. A needle crystal of $(Et_4N)_4$[**4**] was found to occur in orthorhombic non-centrosymmetric space group $Pna2_1$ with $Z = 4$. The absolute structure parameter (Flack parameter) refined as $-0.02(4)$. The asymmetric unit contains one formula weight. The major difference between the two polymorphs of $(Et_4N)_4$[**4**] is the manner of packing the cluster anions in the two lattices. Shiny black plates of $(Et_4N)_3$[**5**]·2DMF resulted from DMF/ether vapor diffusion. The compound crystallizes in monoclinic space group $C2/c$ with $Z = 4$. The asymmetric unit contains one-half cluster anion, one and a half cations, and one DMF solvate molecule disordered over two superimposed positions. Thin black plates of $(Bu_4N)_3$[**5**]·DMF were obtained from DMF/ether vapor diffusion. The compound crystallizes in monoclinic space group $P2/c$ with $Z = 4$. The asymmetric unit consists of one cluster anion and three cations; two of the cations reside on 2-fold axes. Long black plates of $(Et_4N)_3$[**6**]·2DMF were produced by DMF/ether vapor diffusion. The compound crystallizes in monoclinic space group $P2_1/n$ with $Z = 4$. The asymmetric unit contains one formula weight. One sulfur atom of an edt ligand was disordered over two positions and was modeled in a 71:29 occupancy ratio. Crystallographic agreement factors are contained in Tables 1 and 2.[46]

Other Physical Measurements. All measurements were performed under anaerobic conditions. Absorption spectra were recorded with a Varian Cary 50 Bio spectrophotometer. ^{1}H NMR spectra were recorded on a Bruker AM 400 or a Varian Mercury 300 spectrometer. Electrochemical measurements were made with a PAR model 263 potentiostat/galvanostat using a Pt working electrode, 0.1 M $(Bu_4N)(PF_6)$ supporting electrolyte, and a SCE reference. Mössbauer spectra were collected with a constant acceleration spectrometer. Data were analyzed using WMOSS software (WEB Research Co., Edina, MN); isomer shifts are referenced to iron metal at room temperature. EPR spectra were recorded on a Bruker ESP 300-E spectrometer operating at X-band frequencies. Spectral simulations were performed with WIN-EPR SimFonia v. 1.25 software.

Results and Discussion

Cluster Synthesis and Structures. (a) $[(edt)_2M_2FeS_6]^{3-}$. In prior preparations of the M = Mo cluster, the original $[MS_4]^{2-}/FeCl_3/Na_2(edt)$ reaction system of Dahlstrom et al.[36] has been employed**.** In those cases where the mole ratio of reactants was at least partially specified in the preparation of **2**[35,36] and **3**,[35,41] a large excess of the dithiolate was used. We interpret this reaction in terms of the apparent stoichiometry of reaction 1 (M = Mo, W). Accordingly, we have used reaction systems at or near that stoichiometry to afford the air-sensitive compounds $(Et_4N)_3$[**2**] (80%), $(Bu_4N)_3$[**2**] (70%), and $(Et_4N)_3$[**3**] (36%) in the indicated yields. In earlier preparations, yields were not reported. Reaction 1 results in the reduction of M(VI), affording $M^{5+}{}_2Fe^{3+}$ products (vide infra). The clusters may be identified by their absorption spectra in Figure 3, in which bands of **3** are blue-shifted compared to **2**, a usual relationship between strictly analogous molybdenum and tungsten complexes. The spectrum of **2** is in agreement with tabulated spectral data,[34] whereas that of **3** cannot be said to be in close agreement with a published spectrum.[41] The clusters are further identified by their isotropically shifted ^{1}H NMR spectra shown in Figure 4, which consist of four well-resolved equally intense signals. The claim that the edt protons in **2** occur at δ 2.66 in Me_2SO[38] is inconsistent with our result and is otherwise improbable for a paramagnetic cluster. As seen in Figure 5, both clusters undergo reversible electrochemical oxidation, at $E_{1/2} = -0.32$ V for **2** and -0.34 V for **3**. While the potential order is that always found for strictly analogous molybdenum and tungsten complexes,[47] the small separation of only 20 mV is indicative of highly covalent and delocalized bonding at the metal sites. The oxidation is not expected to be localized at the iron site in view of the highly probable instability of Fe(IV) in a tetrathiolate environment. Treatment of **2** with four oxidants ($C_7H_7^+$, TCNQ, I_2, $[Cp_2Fe]^+$) with potentials in the range -0.25 to 0.40 V vs SCE[48] afforded the same product, $[Mo_2S_4(edt)_2]^{2-}$.[42,43] This species is

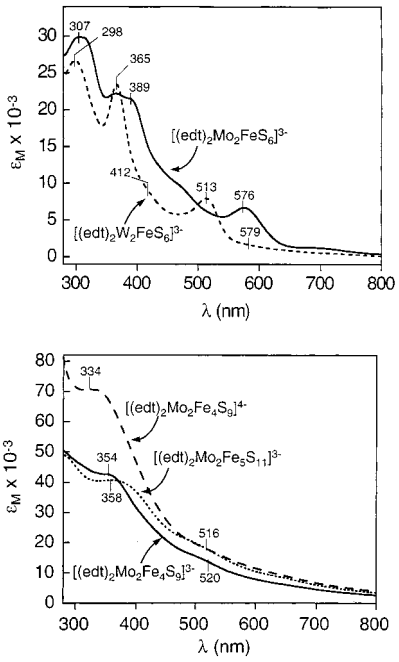

Figure 3. Absorption spectra of $[(edt)_2M_2FeS_6]^{3-}$ (M = Mo, W) in acetonitrile (upper) and $[(edt)_2Mo_2Fe_4S_9]^{4-,3-}$ and $[(edt)_2Mo_2Fe_5S_{11}]^{3-}$ in Me_2SO (lower).

$$2[MS_4]^{2-} + FeCl_3 + 4Na_2(SCH_2CH_2S) \rightarrow [(SCH_2CH_2S)_2M_2FeS_6]^{3-} + Na_2(SCH_2CH_2S)_2 + 2Na_2S + 2NaCl + Cl^- \quad (1)$$

(46) See paragraph at the end of this article for Supporting Information available.

(47) Tucci, G. C.; Donahue, J. P.; Holm, R. H. *Inorg. Chem.* **1998**, *37*, 1602−1608.

(48) Connelly, N. G.; Geiger, W. E. *Chem. Rev.* **1996**, *96*, 877−910.

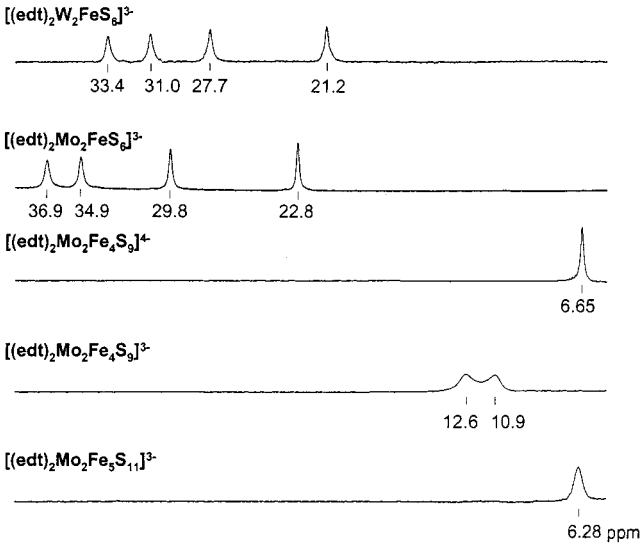

Figure 4. ^{1}H NMR spectra of edt ligands in $[(edt)_2M_2FeS_6]^{3-}$ (M = Mo, W) in acetonitrile and $[(edt)_2Mo_2Fe_4S_9]^{4-,3-}$ and $[(edt)_2Mo_2Fe_5S_{11}]^{3-}$ in Me_2SO.

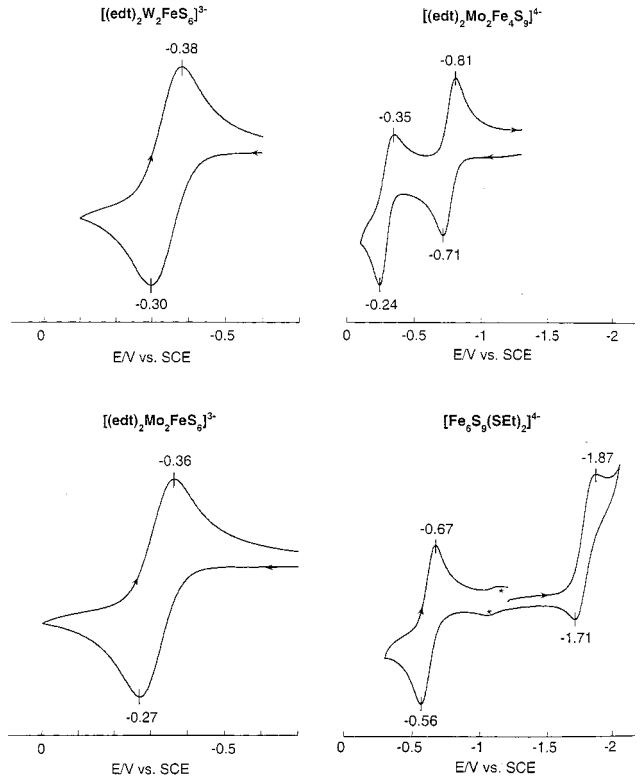

Figure 5. Cyclic voltammograms of $[(edt)_2MFeS_6]^{3-}$ (M = Mo, W) (left) and $[(edt)_2Mo_2Fe_4S_9]^{4-}$ and $[Fe_6S_9(SEt)_2]^{4-}$ (right) at 100 mV/s in Me_2SO solutions. Peak potentials vs SCE are indicated.

evidently formed by oxidation of two of the bridging sulfide atoms in **2**. With ferrocenium, the Et_4N^+ salt containing the anion in the syn configuration was isolated in 55% yield. Oxidation of **3** was examined only with ferrocenium, which afforded the known compound $(Et_4N)_4[W_3Fe_3S_{14}]$[45] (26%).

The X-ray structure of **2** has been determined on several previous occasions. The structure of $(Me_4N)_3$[**2**] was first reported[36] followed by $(Et_4N)_3$[**2**] in space group *Cc*[37,38] and $(Et_4N)_3$[**2**]·$^1/_4$MeCN in space group *Pc*.[39] The two noncentrosymmetric space groups were later revised as *C*2/*c* and

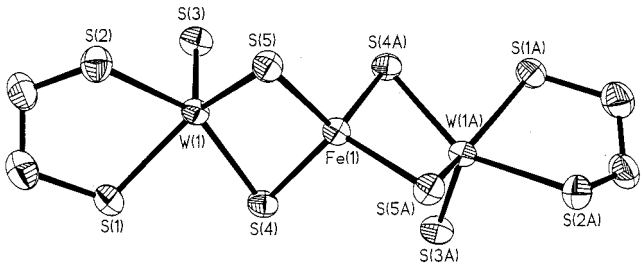

Figure 6. Structure of $[(edt)_2W_2FeS_6]^{3-}$ showing 50% thermal ellipsoids and the atom-labeling scheme; crystallographic C_2 symmetry is imposed. Cluster **2** is isostructural.

Table 3. Selected Interatomic Distances (Å) for Cluster Anion **3**

W(1)−Fe(1)	2.7002(6)	W(1)−S(1)	2.406(2)
W(1)−S(2)	2.425(2)	W(1)−S(3)	2.142(2)
W(1)−S(4)	2.302(2)	W(1)−S(5)	2.303(2)
Fe(1)−S(4)	2.234(2)	Fe(1)−S(5)	2.236(2)

$P2_1/c$, respectively.[40,49] The crystal structure of $(Et_4N)_3$[**3**] has also been reported;[35,41] however, it does not appear in the Cambridge Structural Database (CSD).[50] All of these structures were determined at room temperature. In order to obtain more accurate structural parameters and to facilitate comparison, all structures in this work have been collected at 213 K. Clusters **2** and **3** are isostructural and nearly isometric.[46] The structure of **3** is provided in Figure 6, and selected distances and angles are collected in Table 3. The cluster has an imposed C_2 axis through Fe(1) and consists of two WS_5 square pyramids joined by Fe(1) through four μ_2-S bridges. The torsional angle S(3)−W(1)−W(1A)−S(3A) is 89.7°, and the dihedral angle between the planes S(1,2,4,5) and S(1A,2A,4A,5A) is 87.3°. The W(1) atom is displaced 0.70 Å above the plane S(1,2,4,5) in the direction of apical atom S(3), which is multiply bonded at a distance of 2.142(2) Å. The coordination geometry is similar to that in $[W_2S_4(edt)_2]^{2-}$.[51] The three independent S−Fe−S bond angles (104.4°, 110.5°, 111.0°) are indicative of tetrahedral coordination. The mean Fe−(μ_2-S) bond distance of 2.235 Å is indistinguishable from the mean value of four such bonds in $[Fe_3S_4(SPh)_4]^{3-}$, which contains tetrahedral Fe(III).[16] It follows from the structure that the two edt groups are equivalent but that within each chelate ring the protons are not equivalent even with rapid interconversion of the nonplanar conformations. As already observed (Figure 4), this inequivalence is fully resolved in the ^{1}H NMR spectra of both **2** and **3**.

(b) $[(edt)_2Mo_2Fe_4S_9]^{4-}$. Abbreviated preparations of cluster **4** as the Et_4N^+ salt have been given,[33,35] and in one the mole ratio $[MoS_4]^{2-}$:$FeCl_3$:Na_2(edt) = 1:3.3:19 was specified.[35] Our attempts to reproduce this synthesis afforded **2**, with only a trace amount of **4** detectable by ^{1}H NMR. Thereafter, we devised reaction 2 (n = 4) involving preformed **2** (Figure 2); 4 equiv of thiolate are required to reduce **2** and $FeCl_3$ to the $[Mo_2Fe_4S_9]^0$ core oxidation level of the product. Using the exact stoichiometry of this reaction,

(49) Marsh, R. E. *Acta Crystallogr.* **1997**, *B53*, 317−322.
(50) Allen, F. H.; Kennard, O. *Chem. Des. Autom. News* **1993**, *8*, 1 and 31−35.
(51) Pan, W.-H.; Chandler, T.; Enemark, J. H.; Stiefel, E. I. *Inorg. Chem.* **1984**, *23*, 4265−4269.

$$[(SCH_2CH_2S)_2Mo_2FeS_6]^{3-} + 3FeCl_3 + 3Li_2S + n\text{NaSEt} + (n-3)Cl^- \rightarrow [(SCH_2CH_2S)_2Mo_2Fe_4S_9]^{n-} + 6\text{LiCl} + n\text{NaCl} + (n/2)\text{EtSSEt} \quad (2)$$

we obtained $(Et_4N)_4$[**4**]·5LiCl (60%). We have thus far been unsuccessful in isolating bulk quantities of the cluster salt free of LiCl because of similar solubilities. However, dissolution of this salt in water followed by addition of Bu_4N^+ leads to the isolation of $(Bu_4N)_4$[**4**] (47%), which, unlike $(Et_4N)_4$[**4**], is freely soluble in acetonitrile, allowing separation from LiCl. $(Bu_4N)_4$[**4**] has also been prepared by reaction 2 from $(Bu_4N)_3$[**2**]. Cluster **4** is characterized by an intense absorption band at 334 nm (Figure 3) and a single ^{1}H NMR resonance at δ 6.65 (Figure 4), both in Me_2SO. The absorption spectrum does not resemble that previously reported for **4**.[33,34] The cluster also exhibits two reversible oxidation steps at $E_{1/2} = -0.76$ and -0.30 V in Me_2SO (Figure 5). We do not observe the reported irreversible feature at $E_{1/2} = +0.085$ V vs SCE ($\Delta E_p = 0.27$ V, $i_{pc}/i_{pa} \ll 1$) in DMF.[35]

The published structure of $(Et_4N)_4$[**4**] was collected at room temperature.[33,35] Although no disorder was mentioned in the reported structures, it is noted in the CSD that one cation is disordered and was not retained in the database structure description. In addition, there is a discrepancy in calculated density between the reported and CSD values (1.45 vs 1.59 g/cm^3). These matters suggested that the disordered cation may not have been treated properly and that possibly the 4− cluster charge is incorrect. Therefore, the crystal structure of $(Et_4N)_4$[**4**] was reinvestigated using crystals grown by vapor diffusion; these did not contain LiCl and in this sense resemble the crystals originally investigated.

The compound $(Et_4N)_4$[**4**] was obtained in two crystalline forms. The monoclinic form ($C2/c$) is probably the same as the published room temperature structure for which a = 17.672(2) Å, b = 33.851(4) Å, c = 13.900(3) Å, and β = 135.107(7)° [33,35] (compare with Table 1). However, the cell at 213 K is 3% larger than the room temperature cell, opposite to the normal effect of temperature on a unit cell volume. In the monoclinic form, the cluster resides on a crystallographically imposed 2-fold axis passing through atom S(4) and perpendicular to the Mo_2Fe_4 plane in the structure of Figure 7. One cation is ordered on a general position, one is disordered over two positions with the nitrogen atom on the 2-fold axis, and another disordered cation was modeled as two interpenetrating orientations with one carbon atom located on a 2-fold axis. Thus, the overall cation:anion ratio is 4:1. In the orthorhombic non-centrosymmetric form ($Pna2_1$), all cations and the anion reside on general positions and only one of the cations is (slightly) disordered. The major difference between the two crystalline modifications is in the packing of the anions (not shown). Establishment of cation:anion ratio in the crystal is important, given the existence of a one-electron-oxidized form of **4** (vide infra). Metric parameters of the cluster in the two forms are essentially the same; data for the monoclinic modification are given in Table 4.

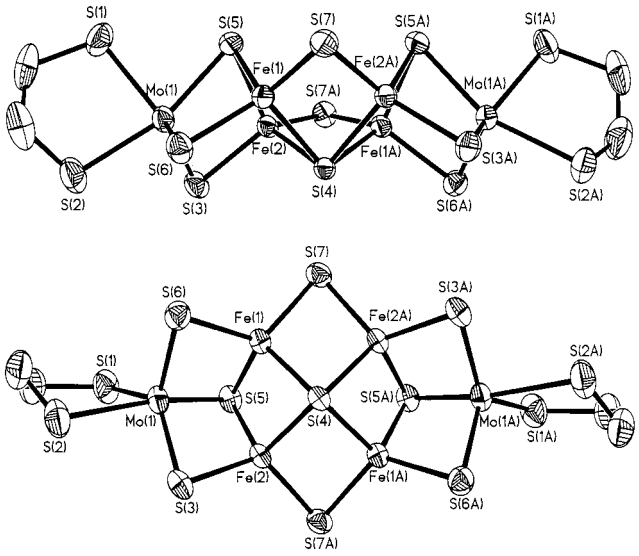

Figure 7. Structure of $[(edt)_2Mo_2Fe_4S_9]^{4-}$ parallel (upper) and perpendicular (lower) to the Mo_2Fe_4 plane; 50% thermal ellipsoids and the atom-labeling scheme are shown. Cluster **5** is essentially isostructural.

Table 4. Selected Interatomic Distances (Å) for Cluster Anions **4**[a] and **5**[b]

	4	**5**		**4**	**5**
Mo(1)−Fe(1)	2.729(2)	2.732(2)	Fe(1)−S(4)	2.333(2)	2.334(3)
Mo(1)−Fe(2)	2.707(2)	2.739(2)	Fe(1)−S(5)	2.284(2)	2.248(5)
Fe(1)−Fe(2)	2.663(2)	2.697(3)	Fe(1)−S(6)	2.257(2)	2.236(5)
Mo(1)−S(1)	2.392(3)	2.370(4)	Fe(1)−S(7)	2.225(2)	2.202(5)
Mo(1)−S(2)	2.485(3)	2.448(4)	Fe(2)−S(4)	2.338(2)	2.331(4)
Mo(1)−S(3)	2.291(3)	2.243(4)	Fe(2)−S(5)	2.275(2)	2.252(5)
Mo(1)−S(5)	2.380(2)	2.375(4)	Fe(2)−S(3)	2.235(2)	2.256(4)
Mo(1)−S(6)	2.263(2)	2.272(4)			

[a] Monoclinic form. [b] Et_4N^+ salt.

The $[Mo_2Fe_4S_9]^0$ core of **4** has the same topology as the core of $[Fe_6S_9(SR)_2]^{4-}$ (Figure 1). It is conceptualized by the fusion of eight nonplanar rhombs, four $MoFeS_2$ and four Fe_2S_2 by edge- and corner-sharing such that a core of C_{2v} symmetry is realized. The core may also be viewed as two cuboidal $MoFe_2S_4$ fragments sharing a common μ_4-S(4) atom such that the vacant metal sites that would complete a cubane unit are on the same side of the Mo_2Fe_4 plane. These six metal atoms are nearly coplanar (mean deviation 0.06 Å) as are μ_2-S(3,3A,6,6A) and μ_4-S(4) (mean deviation 0.02 Å); the distance between the planes is 1.3 Å. Relative to the Mo_2Fe_4 plane, the atoms μ_2-S(7,7A) and μ_3-S(5,5A) are located at distances of 0.7 and 1.7 Å, respectively, on the opposite side from μ_4-S(4). The iron atoms exhibit distorted tetrahedral coordination; bond lengths increase in the expected order Fe−(μ_2-S) > Fe−(μ_3-S) > Fe−(μ_4-S). The stereochemistry at the molybdenum sites is approximately trigonal bipyramidal with S(2) and S(5) at the axial positions (S(2)−Mo(1)−S(5) = 158.8°). Note that the terminal sulfido ligand has been lost in the conversion of **2** to **4**. The Mo(edt)chelate rings adopt an envelope configuration and are canted with respect to the metal plane, as shown by the dihedral angle of 77.6° between the planes S(1)−Mo(1)−S(2) and Mo(1)−Fe(1)−Fe(2). The axial Mo(1)−S(2) bond is 0.093 Å longer than equatorial Mo(1)−S(1), apparently because of the repulsion of equatorial atoms S(3,6). The overall structure

of C_2 symmetry affords two sets of inequivalent protons under rapid ring conformational interchange. However, their resonances are not resolved at ambient temperature (Figure 4).

Although of the same charge and with related core structures, clusters **1** and **4** exhibit contrasting electrochemical behavior (Figure 5). The former undergoes a reduction at −1.79 V and an oxidation at −0.62 V whereas the latter, as already noted, shows two successive oxidations at −0.76 and −0.30 V. The only possibly corresponding steps in terms of electronic properties of the products are the two oxidations differing by 0.14 V. No cluster of the type $[Fe_6S_9(SR)_2]^{3-}$ has yet been isolated. In this work, we have examined the oxidation reactions of **4**.

(c) $[(edt)_2Mo_2Fe_4S_9]^{3-}$. Noting the facile one-electron oxidation of **4** at −0.76 V, the cluster in DMF was treated with 1 equiv of $C_7H_7^+$. Oxidized cluster **5** was isolated as $(Et_4N)_3$[**5**]·2DMF (65%). Alternatively, $(Bu_4N)_3$[**5**] (53%) was obtained directly from reaction 2 by adjusting the amount ($n = 3$) of reducing equivalents. The cluster exhibits an intense absorption feature at 354 nm (Figure 3). The structures of **4** and **5** are essentially congruent (Figure 7). The appearance of two equally intense features in the ^{1}H NMR spectrum (Figure 4) is consistent with this structural relationship. Bond distances and angles are compared in Table 4, from which it is seen that few dimensions undergo statistically significant changes at the 3σ level. However, there appears a trend toward shorter Mo−S and Fe−S distances upon oxidation, suggesting that an electron is removed from a delocalized antibonding orbital. There is also an indication that the Fe(1)−Fe(2) side of the Fe_4 rectangle increases by 0.034 Å and the Fe(2)−Fe(1A) side decreases by 0.041 Å upon oxidation.

The near-equivalence of corresponding metric features is indicative of static disorder of odd-electron **5** in the crystal or a delocalized electronic structure. As found by Mössbauer spectroscopy (vide infra), the latter is the more probable, consistent with the usual behavior of Fe−S and Mo−Fe−S clusters. Because of the small differences in metric parameters between **4** and **5**, we cannot ascertain with certainty whether the original description of the structure assigned to the 4− cluster[33] is actually that or instead it is the structure of 3− or a mixture of 3− and 4− clusters, conceivable scenarios given the oxidative sensitivity of authentic **4**. Whatever the case, the atom connectivity as originally described is certainly correct and the bond distances and angles at room temperature are within ca. 0.05 Å and 5°, respectively, of the values found in this work. However, in the reported structure[33,35] the Mo−S and Fe−S distances are *shorter* than the values found here for **4**, yet they are comparable with those for **5**.

(d) $[(edt)_2Mo_2Fe_5S_{11}]^{3-}$. Attempted two-electron oxidation of **4** or one-electron oxidation of **5** did not yield $[(edt)_2Mo_2Fe_4S_9]^{2-}$ expected from cyclic voltammetry (Figure 5). Instead, a cluster with a new topology was isolated as $(Et_4N)_3$[**6**]·2DMF (44%) upon oxidation of **4** with 2 equiv of ferrocenium in DMF. The cluster exhibits an absorption spectrum similar to that of **5** (Figure 3) and a single broad

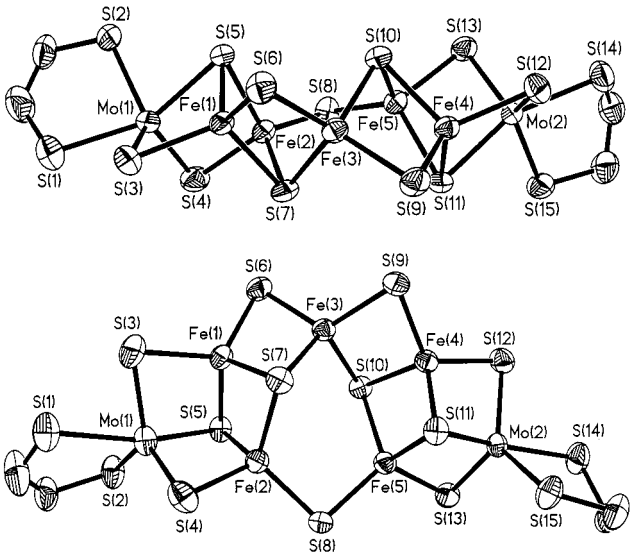

Figure 8. Structure of $[(edt)_2Mo_2Fe_5S_{11}]^{3-}$ approximately parallel (upper) and perpendicular (lower) to the Mo_2Fe_5 plane; 50% thermal ellipsoids, the atom-labeling scheme, and the majority position of atom S(1) are shown.

Table 5. Selected Interatomic Distances (Å) for Cluster Anion **6**

Mo(1)−Fe(1)	2.7367(9)	Mo(2)−Fe(4)	2.7174(8)
Mo(1)−Fe(2)	2.7732(9)	Mo(2)−Fe(5)	2.7851(8)
Fe(1)−Fe(2)	2.724(1)	Fe(4)−Fe(5)	2.712(1)
Mo(1)−S(1)	2.431(2)	Mo(2)−S(14)	2.428(2)
Mo(1)−S(2)	2.345(2)	Mo(2)−S(15)	2.365(2)
Mo(1)−S(3)	2.245(2)	Mo(2)−S(12)	2.277(2)
Mo(1)−S(4)	2.259(2)	Mo(2)−S(13)	2.226(2)
Fe(1)−S(5)	2.256(2)	Fe(4)−S(11)	2.249(2)
Fe(1)−S(7)	2.245(2)	Fe(4)−S(10)	2.237(2)
Fe(1)−S(3)	2.247(2)	Fe(4)−S(12)	2.230(2)
Fe(1)−S(6)	2.206(2)	Fe(4)−S(9)	2.204(2)
Fe(2)−S(5)	2.240(2)	Fe(5)−S(11)	2.248(2)
Fe(2)−S(7)	2.306(2)	Fe(5)−S(10)	2.307(2)
Fe(2)−S(4)	2.266(2)	Fe(5)−S(13)	2.292(2)
Fe(2)−S(8)	2.216(2)	Fe(5)−S(8)	2.201(2)
Fe(3)−S(7)	2.293(2)	Fe(3)−S(10)	2.293(2)
Fe(3)−S(6)	2.211(2)	Fe(3)−S(9)	2.217(2)

^{1}H NMR resonance of δ 6.28 in Me_2SO (Figure 4). Its structure, presented in Figure 8 with metric data available in Table 5, consists two $MoFe_2S_4$ cuboidal fragments vertex-bridged by μ_2-S(8) and edge-bridged by two Fe_2S_2 rhombs having Fe(3) in common. The structure contains seven μ_2-S and four μ_3-S atoms. The five metal atoms (Mo(1,2), Fe(1,3,4)) are nearly coplanar (mean deviation 0.06 Å). Although there is no crystallographically imposed symmetry, cluster **6** has a pseudo-C_2 axis passing through Fe(3) and S(8), placing the $MoFe_2S_4$ cuboidal cavities on opposite sides of the cluster. As in **4** and **5**, iron atoms occur as distorted tetrahedral FeS_4 units and the molybdenum atoms have irregular trigonal bipyramidal coordination. The nonplanar central Fe_3S_3 ring is reminiscent of that in $[Fe_3(SR)_3X_6]^{3-}$,[52] where it is planar, and that in $[Fe_4(SR)_{10}]^{2-}$,[53] where it is not. The Fe_4S_5 fragment Fe(1,3,4,5)S(6,7,9−11), consisting of one vertex-shared and two edge-shared Fe_2S_2 rhombs, has been observed in the cluster $[Na_2Fe_{18}S_{30}]^{8-}$ whose cyclic

(52) Whitener, M. A.; Bashkin, J. K.; Hagen, K. S.; Girerd, J.-J.; Gamp, E.; Edelstein, N.; Holm, R. H. *J. Am. Chem. Soc.* **1986**, *108*, 5607−5620.
(53) Hagen, K. S.; Stephan, D. W.; Holm, R. H. *Inorg. Chem.* **1982**, *21*, 3928−3936.

Table 6. Zero-Field Mössbauer Parameters at 4.2 K

cluster	δ (mm/s)	ΔE_Q (mm/s)	%
$[Fe_6S_9(SEt)_2]^{4-}$ [a]			
A	0.45	0.70	75
	0.29	0.57	25
B	0.42	0.75	70
	0.36	0.45	30
$[Fe_6S_9(SCH_2Ph)_2]^{4-}$ [a,b]	0.45[c]	0.70	75
	0.29[c]	0.57	25
$[Fe_6S_9(SBu^t)_2]^{4-}$ [d]	0.41[c]	0.72	66
	0.40[c]	0.43	33
$[Fe_4S_4(SEt)_4]^{2-}$ [a]	0.44	1.19	
$[Fe_4S_4(SEt)_4]^{3-}$ [a]	0.59	1.64	
$[(edt)Mo_2FeS_6]^{3-}$ [a]	0.33	0.84	
$[(edt)_2Mo_2Fe_4S_9]^{4-}$ [a]	0.45	1.04	
$[(edt)_2Mo_2Fe_4S_9]^{3-}$ [a,e]	0.40	1.27	

[a] Et_4N^+ salt. [b] Reference 17. [c] 0.12 mm/s added to reported shift to adjust to iron metal reference at room temperature. [d] $Me_3NCH_2Ph^+$ salt, MeOH solvate; ref 14. [e] 2DMF solvate.

structures are built up entirely of shared rhombs.[54,55] However, no cluster with the complete topology of **5** has been encountered previously.

Electron Distribution and Oxidation States. As with virtually all other heterometal iron−sulfur clusters, **2**−**6** pose the problem of electron distribution and the assignment of oxidation states. To investigate this matter, zero-field ^{57}Fe Mössbauer spectra of **2** and **4**−**6** have been measured at 4.2 K; parameters are summarized in Table 6. Our results do not agree with the parameters quoted by Zhang et al.[35] for **2** and **4** when their isomer shifts are corrected by addition of 0.12 mm/s to the iron metal reference at room temperature used in this study. For tetrahedral $Fe^{II}S_4$ and $Fe^{III}S_4$ units, isomer shifts are typically 0.60−0.70 and 0.20−0.35 mm/s at 4.2 K, respectively.[56] Intermediate oxidation states are present in the clusters $[Fe_4S_4(SEt)_4]^{2-}$ ($Fe^{2.5+}$) and $[Fe_4S_4(SEt)_4]^{3-}$ ($Fe^{2.25+}$). Cluster **2** exhibits a very broad quadrupole doublet (not shown, line width $\Gamma > 0.60$ mm/s) indicative of a paramagnetic ground state. The average isomer shift and quadrupole splitting (0.33 and 0.84 mm/s, respectively) are strongly suggestive of an Fe^{3+} site. As the Mössbauer spectrum remains broad up to room temperature, preventing us from obtaining more information about the electronic structure, we have recorded the EPR spectrum at 4.2 and 45 K. The 4.2 K spectrum, shown in Figure 9, has the principal g values 5.02, 2.89, and 1.84 and is characteristic of an $S = {}^3/_2$ ground state with a positive zero-field splitting and rhombicity parameter $E/D = 0.18$. The ground state apparently originates from antiferromagnetic coupling of the $S = {}^5/_2$ spin of the central Fe^{3+} ion with two reciprocally parallel-oriented $S = {}^1/_2$ spins of the outer Mo^{5+} sites. Cluster **3** is expected to have an analogous ground state.

Prior to considering clusters **4**−**6**, we examine the Mössbauer spectra of the topologically related clusters **1** (Figure 1). Previously, the spectra of $[Fe_6S_9(SR)_2]^{4-}$ with R = Bu^t [14] and CH_2Ph[17] have been briefly described (Table 6). The $[Fe_6S_9]^{2-}$ core requires the formal assignment $[(Fe^{3+})_4(Fe^{2+})_2]$. If the cluster is valence-localized, the Mössbauer spectrum would consist of a pair of quadrupole doublets in a 2:1 intensity ratio, with the isomer shift of the majority iron lower than that of the minority iron. The spectrum of $[Fe_6S_9(SEt)_2]^{4-}$ in Figure 10B is relatively broad, confirming the presence of inequivalent iron sites. The spectrum can be simulated using a pair of quadrupole doublets in an approximate 2:1 ratio. Two pairs of quadrupole doublets, A and B in Table 6, can be used in the simulation.[57] For both assignments, the isomer shift of the majority iron is larger than that for the minority iron, in contrast to the expectation from valence localization. Therefore, the assignment $[(Fe^{3+})_2(Fe^{2.5+})_4]$ better fits the Mössbauer data. Note that the isomer shift of the majority iron (0.45 and 0.42 mm/s in A and B, respectively) is very close to that for $[Fe_4S_4(SEt)_4]^{2-}$ (0.44 mm/s).

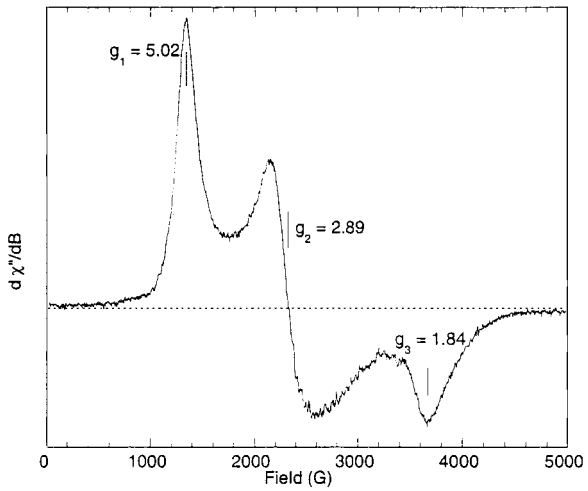

Figure 9. EPR spectrum of a 0.8 mM solution of $(Et_4N)_3[(edt)_2Mo_2FeS_6]$ in DMF at 4 K: microwave power 0.1 mW, microwave frequency 9.43 GHz, modulation amplitude 9.7 G, modulation frequency 100 MHz. Principal g values are indicated.

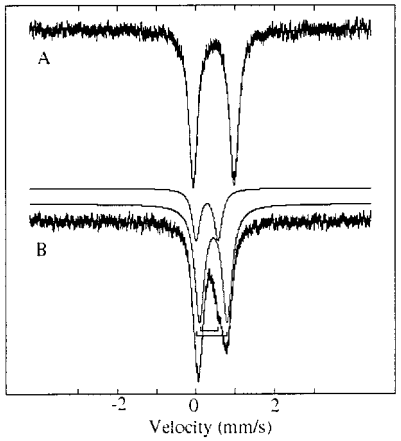

Figure 10. Zero-field Mössbauer spectra at 4.2 K for solid samples of $(Et_4N)_4[(edt)_2Mo_2Fe_4S_9]$ (A) and $(Et_4N)_4[Fe_6S_9(SEt)_2]$ (B). Solid lines through the spectra represent simulations using quadrupole doublets with the parameters in Table 6. Brackets below spectrum B represent the positions of the lines in the doublet assignment B (see text and Table 6). The two doublets for simulation A are also represented above spectrum B.

(54) You, J.-F.; Snyder, B. S.; Papaefthymiou, G. C.; Holm, R. H. *J. Am. Chem. Soc.* **1990**, *112*, 1067−1076.
(55) You, J.-F.; Papaefthymiou, G. C.; Holm, R. H. *J. Am. Chem. Soc.* **1992**, *114*, 2697−2710.
(56) Münck, E. Aspects of ^{57}Fe Mössbauer Spectroscopy. In *Physical Methods in Inorganic and Bioinorganic Chemistry*; Que, L., Jr., Ed.; University Science Books: Sausalito, CA, 2000.

The spectrum of cluster **4** in Figure 10A consists of a unique quadrupole doublet whose narrow line width (Γ = 0.27 mm/s) indicates equivalence of the four iron sites. The isomer shift and quadrupole splitting (0.45 and 1.04 mm/s, respectively) are practically identical to those of $[Fe_4S_4(SEt)_4]^{2-}$ and other $[Fe_4S_4]^{2+}$ clusters with terminal thiolate ligation.[58,59] This coincidence leads us to the oxidation state assignment $[(Mo^{4+})_2(Fe^{2.5+})_4]$. The spectrum of cluster **5** (not shown) shows a broad quadrupole doublet whose smaller isomer shift (0.40 mm/s) is consistent with this cluster being an oxidation product of **4**. Given the isomer shift difference of 0.15 mm/s caused by one electron in the pair $[Fe_4S_4(SEt)_4]^{2-,3-}$, the relatively small shift difference of 0.05 mm/s between **4** and **5** suggests that the hole created in oxidation is delocalized extensively over the larger Fe_4S_9 cluster fragment. At temperatures between 4.2 and 200 K, cluster **6** shows an asymmetric quadrupole doublet (spectra not shown) with an average isomer shift of 0.35 mm/s, indicating a higher average oxidation state for iron than in **4** and **5**. While this value is close to that (0.33 mm/s) for the Fe^{3+} site in **2**, the lack of resolution in the spectra prevents us from obtaining more definite information about the individual oxidation states of the iron sites.

Summary. The following are the principal results and conclusions from this investigation.

1. Detailed syntheses have been developed for the Et_4N^+ and Bu_4N^+ salts of $[(edt)_2M_2FeS_6]^{3-}$ (M = Mo, W) and $[(edt)_2Mo_2Fe_4S_9]^{4-}$, clusters described earlier but with only cursory preparations given. The trinuclear clusters are obtained from the self-assembly systems $2[MS_4]^{2-}/FeCl_3/4Na_2(edt)$ in methanol. Accurate structures of $[(edt)_2M_2FeS_6]^{3-}$ substantiate earlier descriptions based on less extensive room temperature data. Mössbauer and EPR spectroscopic data support the description $2Mo^{5+} + Fe^{3+}$.

2. The assembly systems $[(edt)_2Mo_2FeS_6]^{3-}/3FeCl_3/3Li_2S/n$NaSEt in methanol:acetonitrile afford the hexanuclear clusters $[(edt)_2Mo_2Fe_4S_9]^{n-}$ (n = 3, 4), which are electrochemically coupled by a redox step at −0.76 V. The 3− cluster is also obtained by chemical oxidation using tropylium ion. The assembly reactions are notable in that they involve, in effect, the stoichiometric addition of iron and sulfide to the trinuclear precursor in Summary paragraph 1 with attendant bond rearrangment.

3. The clusters in Summary paragraph 2 are essentially isostructural and contain two cuboidal $MoFe_2S_4$ fragments bridged by a μ_4-S atom in $[Mo_2Fe_4S_9]^{0,1+}$ with five-coordinate molybdenum and tetrahedral iron sites. The cluster bridging pattern ($6(\mu_2\text{-S}) + 2(\mu_3\text{-S}) + \mu_4\text{-S}$) is precedented only in $[Fe_6S_9(SR)_2]^{4-}$. The only clusters with the same sulfide content as FeMoco are $[(edt)_2Mo_2Fe_4S_9]^{3-,4-}$ and $[Fe_6S_9(SR)_2]^{4-}$.

4. Reaction of $[(edt)_2Mo_2Fe_4S_9]^{n-}$ with 1 (n = 3) or 2 (n = 4) equiv of ferrocenium ion yields the cluster $[(edt)_2Mo_2Fe_5S_{11}]^{3-}$, which has the molybdenum and iron site stereochemistry of its precursors and the $[Mo_2Fe_5S_{11}]^{1+}$ core with a bridging pattern ($7(\mu_2\text{-S}) + 4(\mu_3\text{-S})$) not previously encountered.

5. From ^{57}Fe isomer shifts, the (mean) iron oxidation state in the clusters increases in the order $[(edt)_2Mo_2Fe_4S_9]^{4-} < [(edt)_2Mo_2Fe_4S_9]^{3-} \approx [Fe_6S_9(SR)_2]^{4-} < [(edt)_2Mo_2Fe_5S_{11}]^{3-}$.

With the syntheses and properties of the foregoing clusters now well characterized and prior descriptions of these matters clarified or corrected, attention is being directed to two aspects: (i) formation of new clusters of comparable nuclearity and sulfur content that may be accessible from related assembly systems; (ii) the possibility of forming higher nuclearity structures by metal ion incorporation of exisiting clusters such as $[(edt)_2Mo_2Fe_4S_9]^{4-,3-}$.

Acknowledgment. This research was supported by NIH Grant 28846.

Supporting Information Available: X-ray crystallographic data for the seven compounds in Tables 1 and 2. This material is available free of charge via the Internet at http://pubs.acs.org.

IC0201250

(57) There is an apparent discrepancy in the Mössbauer parameters determined for the clusters $[Fe_6S_9(SR)_2]^{4-}$ (R = Bu^t, CH_2Ph; Table 6), but a possible reconciliation follows from our analysis of the spectrum of $[Fe_6S_9(SEt)_2]^{4-}$. Assignment A is close to the parameters reported for $(Me_3NCH_2Ph)_4[Fe_6S_9(SBu^t)_2]\cdot$MeOH while assignment B is close to the values reported for $(Et_4N)_4[Fe_6S_9(SCH_2Ph)_2]$. Therefore, it is likely that two assignments were also possible in the original Mössbauer analysis of these two compounds. The available data do not allow us to determine which of the two assignments is correct.

(58) Frankel, R. B.; Averill, B. A.; Holm, R. H. *J. Phys. (Paris)* **1974**, *36* (C5), 107−111.

(59) Silver, J.; Fern, G. R.; Miller, J. R.; McCammon, C. A.; Evans, D. J.; Leigh, G. J. *Inorg. Chem.* **1999**, *38*, 4256−4261.